Supporting information

Post-synthesis deposition of mesoporous niobic acid with improved thermal stability by kinetically controlled sol-gel overcoating

Yuan-Peng Du, Florent Héroguel, Xuan Trung Nguyen and Jeremy S. Luterbacher*

Laboratory of Sustainable and Catalytic Processing, Institute of Chemical Sciences and Engineering, École Polytechnique Fédérale de Lausanne (EPFL), CH-1015 Lausanne, Switzerland.

*Corresponding author: jeremy.luterbacher@epfl.ch.

Table of Contents

1. Supporting figures

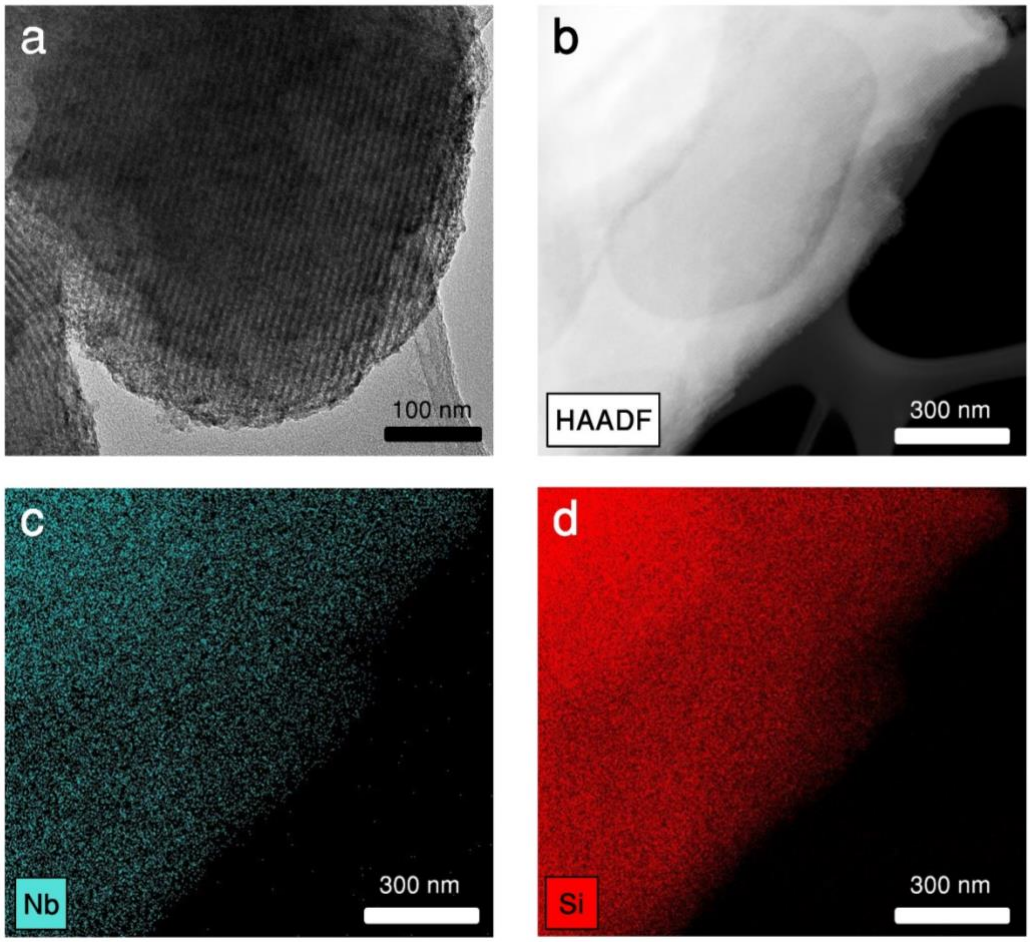

Figure S1. Microscope images of $2Nb_2O_5$@SBA-15 under (a) regular TEM bright field and (b) STEM HAADF mode with EDX mapping of (c) Nb and (d) Si.

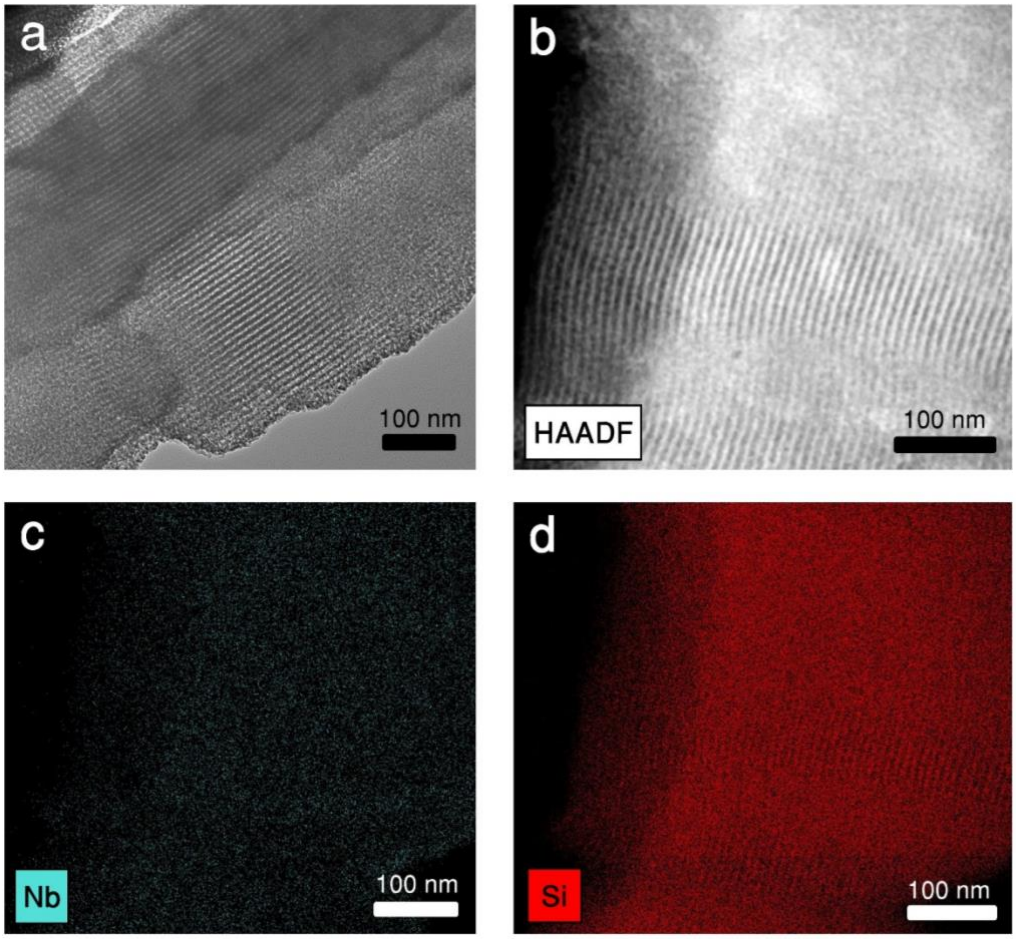

Figure S2. Microscope images of $3Nb_2O_5$@SBA-15 under (a) regular TEM bright field and (b) STEM HAADF mode with EDX mapping of (c) Nb and (d) Si.

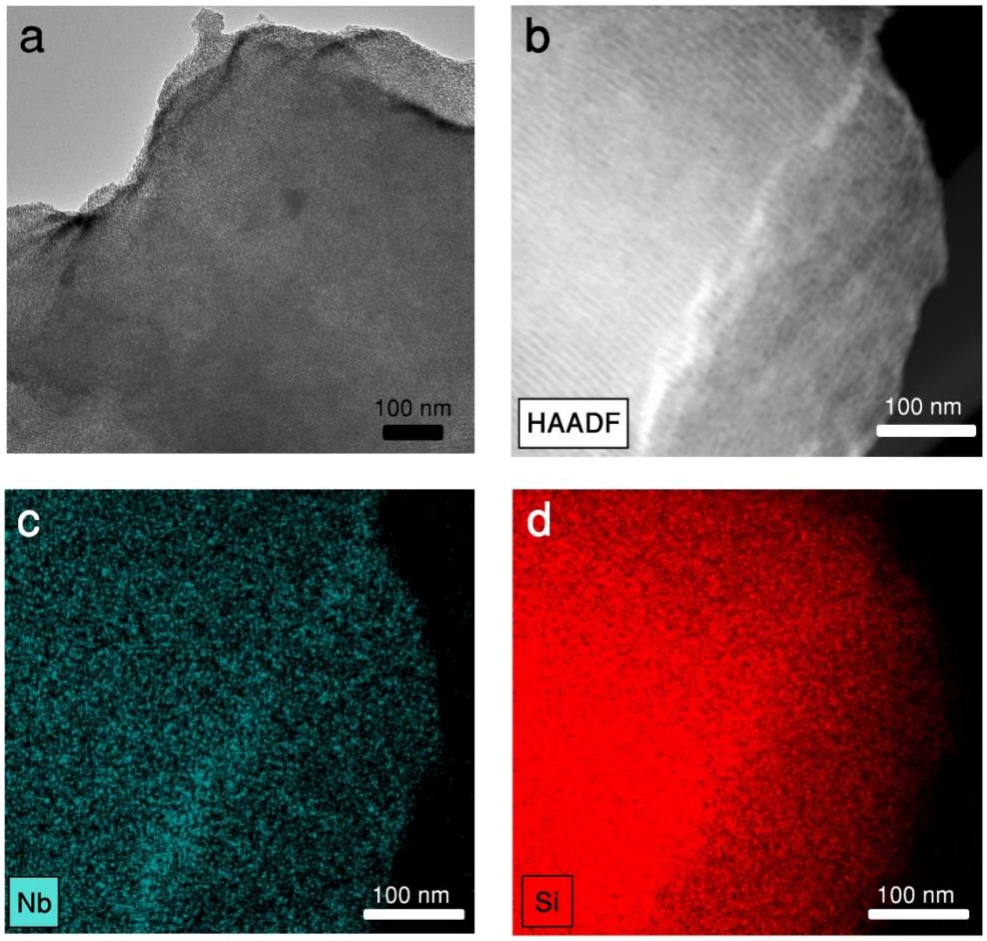

Figure S3. Microscope images of $4Nb_2O_5$@SBA-15 under (a) regular TEM bright field and (b) STEM HAADF mode with EDX mapping of (c) Nb and (d) Si.

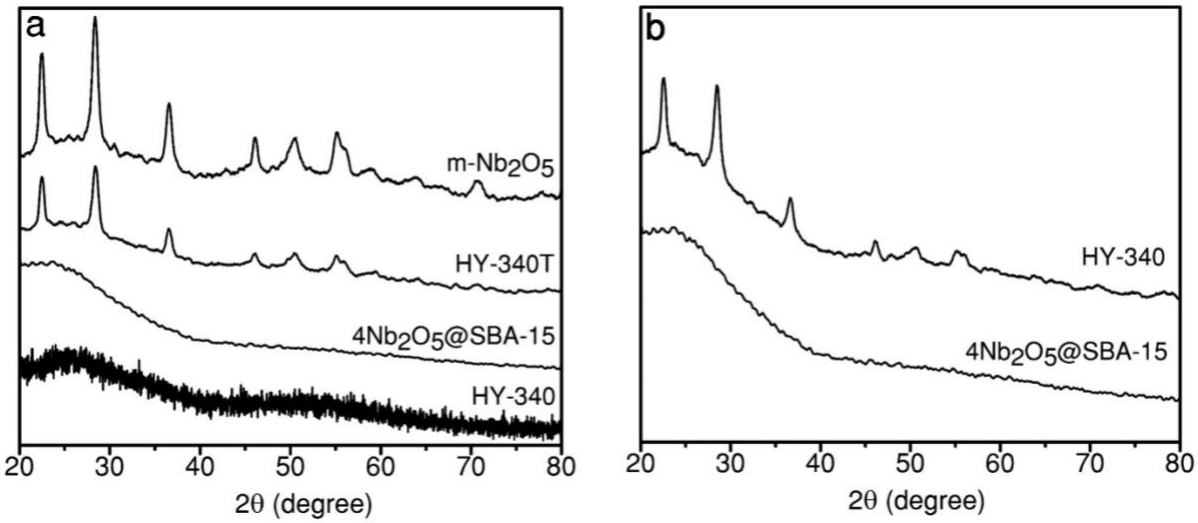

Figure S4. XRD analyses of (a) bulk niobia and overcoated catalysts and, (b) HY-340 and $4Nb_2O_5$@SBA-15 after three catalyst regenerations. The crystal phases of m-Nb_2O_5, HY340T and regenerated HY-340 were identified as a pseudo-hexagonal phase in accordance with past reports.[1] All data were smoothed using the adjacent-averaging method with a 40 point window.

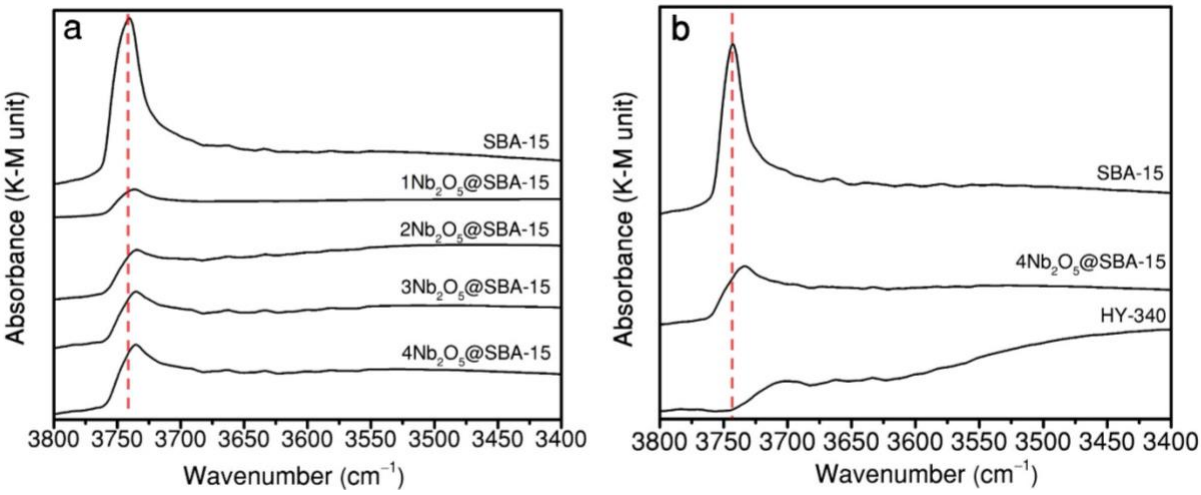

Figure S5. (a) FTIR spectra of dried uncoated and overcoated SBA-15 in the OH region. SBA-15 displays a strong Si–OH stretching peak at 3745 cm^{-1}. A slight increase of intensity and redshift of this peak can be observed for overcoated samples because of the association with the Nb–OH band. This band can be seen in the FTIR spectra of (b) SBA-15, HY-340, and $4Nb_2O_5$@SBA-15. All the data were smoothed using the adjacent-averaging method with a 40 point window.

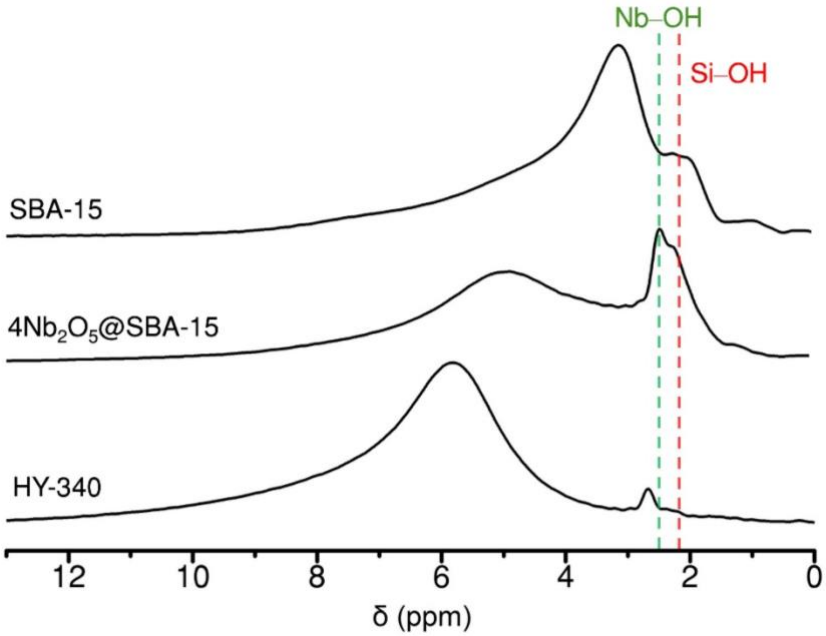

Figure S6. ^{1}H ssNMR spectra of SBA-15, $4Nb_2O_5$@SBA-15 and HY-340. For SBA-15, the peak at 2.2 ppm was assigned to isolated silanols and the broad peak from 3 ppm to 8 ppm is attributed to strongly physisorbed water and hydrogen bonded silanols.[2] The isolated silanol peak can still be observed for $4Nb_2O_5$@SBA-15 and partially overlaps with a peak at 2.4 ppm, which was assigned to isolated Nb–OH.[3]

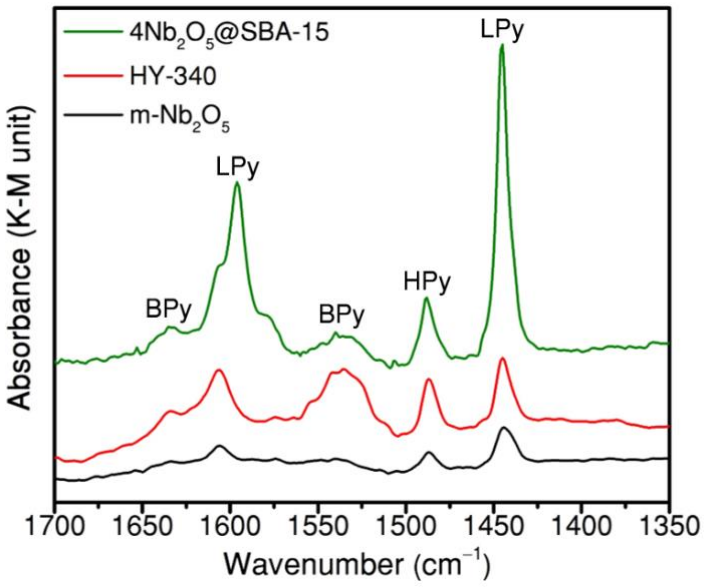

Figure S7. DRIFT-Pyridine spectra of overcoated and bulk niobia catalysts recorded at 323 K. BPy, LPy and HPy denote pyridine adsorbing on Brønsted acid sites, pyridine adsorbing on Lewis acid site and H-bonded pyridine, respectively.[4]

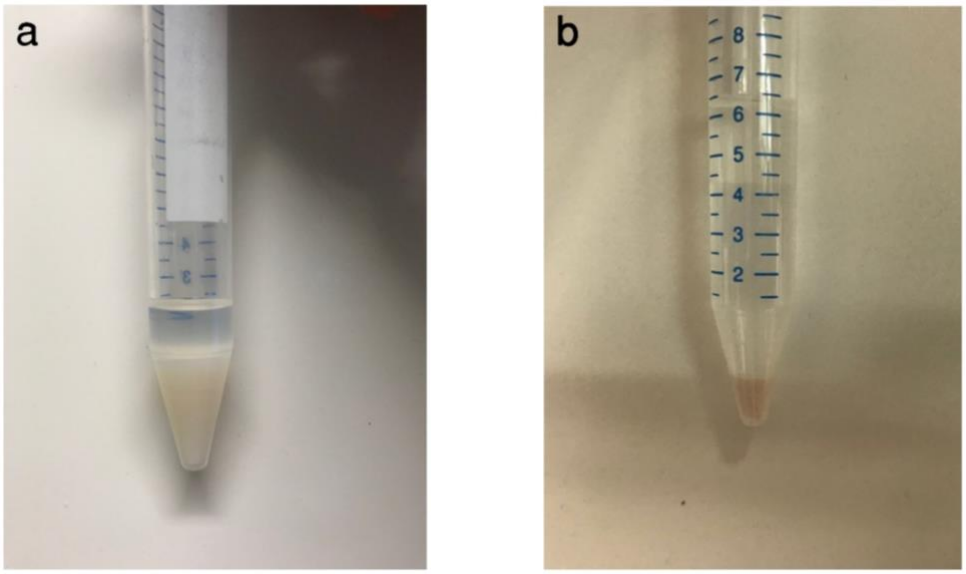

Figure S8. Spent $4Nb_2O_5$@SBA-15 (a) at 84% and (b) at 100% conversion.

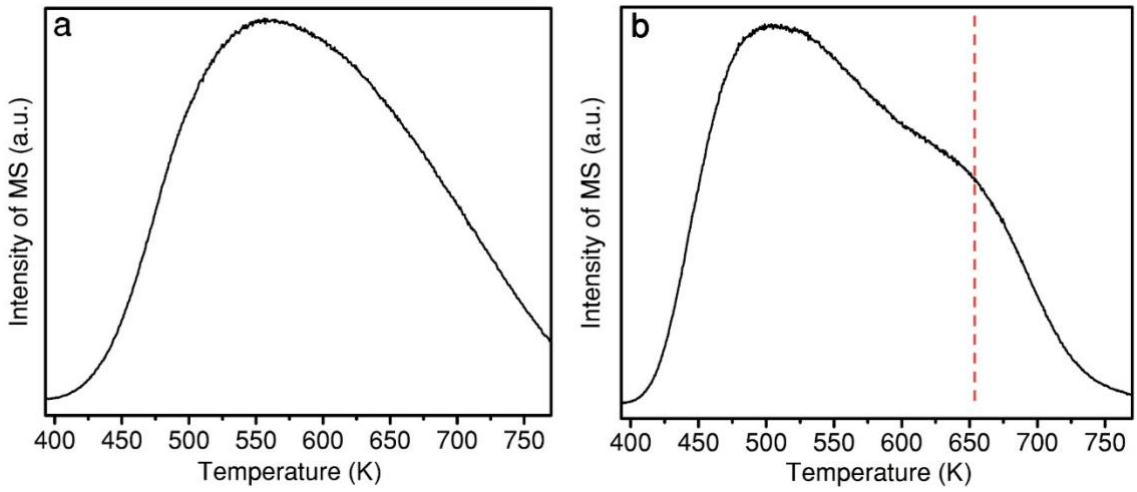

Figure S9. Ammonia TPD result for (a) $4Nb_2O_5$@SBA-15 and (b) HY-340. HY-340 has a desorption band at 653 K, which can be assigned to strong Brønsted acid sites.[5]

2. Assessment of the presence of mass transfer limitations

HY-340 had a lower activity in Friedel-Crafts alkylation and a lower selectivity in xylose dehydration. To confirm that these observations were not due to mass transfer limitations, we performed stirring tests to exclude the effect of any external mass transfer and used the Weisz-Prater criterion to exclude the effects of internal mass transfer limitations. Specifically, we performed control experiments with a faster and slower stirring rate. We observed 57% (550 rpm) and 57% (700 rpm) conversion at 3 h for Friedel-Crafts alkylation and 42% (550 rpm) and 41% (700 rpm) conversion at 30 min for xylose dehydration. Because no significant external mass transfer limitation was observed, the concentration at the surface of the catalyst (C_{AS}) was assumed to be identical as the bulk concentration. Following this, we assessed any internal effects by using the Weisz-Prater criterion (which, if respected, indicates negligible internal mass transfer limitations):

$$\frac{r_{obs}(\mathrm{R}_p)^2}{D_{TA}^e C_{AS}} < 1$$

Where:

r_{obs} is the observed reaction rate per unit volume of catalyst (mol·s^{-1}·cm^{-3})

R_p is the spherical particles radius (cm)

D_{TA}^e is the effective transition diffusivity (cm^2·s^{-1})

C_{AS} is the concentration at the surface of the catalyst particle (mol·cm^{-3}) which was set equal to the bulk concentration.

The particle radius of HY-340 was estimated using an optical microscope. The reaction rates were obtained experimentally. For Friedel-Crafts alkylation, the initial rate shown in Figure 6 was directly used for the calculation. For xylose dehydration, we performed the reaction with a shorter reaction time (10 min) to obtained an average reaction rate at low conversion (14 %).

Bulk diffusivities of benzyl alcohol in anisole and xylose in water, were calculated using the Wilke-Chang equation:[6]

$$D_{AB} = 7.4 \times 10^{-8} \frac{T}{\mu} \frac{(x\, M_B)^{1/2}}{V_A^{0.6}}$$

Where μ is the solvent dynamic viscosity, T is the reaction temperature (K), M_B is the molecular weight of solvent, x is the association parameter (taken as 1) and V_A is the molar volume at the boiling point of the solute. The solvent dynamic viscosities were obtained from the literature (0.908 mPa·s for anisole and 0.89 mPa·s for water).[7,8] In the absence of data at the reaction temperature, the dynamic viscosity at a lower temperature was used. This simplification leads to an underestimation of D_{AB}, and hence, an overestimation of the Weisz-Prater criterion, ensuring that no mass transfer effects are present. Using the method reported by Sastri, V_A was calculated as 124 $cm^3 \cdot mol^{-1}$ for benzyl alcohol and 120 $cm^3 \cdot mol^{-1}$ for xylose (furanose structure).[9] The D_{AB} coefficient was then calculated as $1.89 \cdot 10^{-5}$ for Friedel-Crafts alkylation and $7.84 \cdot 10^{-6}$ for xylose dehydration.

The pore diffusivity can be determined by the equation below:[6]

$$\frac{D_{AB,pore}}{D_{AB}} = (1-\lambda)^4$$

$$\text{Where } \lambda = \frac{d_s}{d_p}$$

The solute diameter (d_s) was calculated using the MarvinSketch software and the average pore diameter of HY-340 (d_p) was determined by using the BJH adsorption analysis. The internal diffusivity within the pores of the catalyst particles with respect to that of the bulk for liquid phase conditions was determined with this equation and summarized in Table S1.

Table S1. Physical properties of solute and HY-340

Parameter	Description	Unit	Friedel-Crafts	Xylose

			alkylation	dehydration
d_s	solute diameter	nm	0.26	0.45
d_p	pore diameter	nm	6	6
$\frac{D_{AB,pore}}{D_{AB}}$	variation of diffusivity	-	0.837	0.732
$D_{AB,pore}$	pore diffusivity	$cm^2 \cdot s^{-1}$	$1.58 \cdot 10^{-5}$	$5.74 \cdot 10^{-6}$

The effective diffusivity was subsequently calculated using the porosity (ε) and the tortuosity (τ):

$$D_{TA}^{e} = D_{AB}^{e} = \frac{\varepsilon}{\tau} D_{AB,pore}$$

In the absence of experimental data, ε and τ can be estimated according to Davis et al.[10] The ε is 0.5 and the τ is 4 for both reactions. The D_{TA}^{e} was then calculated and the Weisz-Prater criterion was estimated (Table S2).

Table S2. Summary of Weisz-Prater criterion.

Parameter	Description	Unit	Friedel-Crafts alkylation	Xylose dehydration
r_{obs}	observed rate of reaction	$mol \cdot cm^{-3} \cdot s^{-1}$	$2.04 \cdot 10^{-6}$	$8.7 \cdot 10^{-7}$
R_p	particle radius	cm	$2 \cdot 10^{-3}$	$2 \cdot 10^{-3}$
D_{TA}^{e}	Effective diffusivity	$cm \cdot s^{-1}$	$1.98 \cdot 10^{-6}$	$7.18 \cdot 10^{-7}$
C_{AS}	surface concentration	$mol \cdot cm^{-3}$	$4.34 \cdot 10^{-4}$	$2.5 \cdot 10^{-4}$

	Weisz-Prater criterion		$9.5 \cdot 10^{-3}$	$1.9 \cdot 10^{-2}$

Since the calculated criterions were systematically several orders of magnitude below unity, we concluded that the reactions we ran were free of internal diffusion limitation. Although the observed rates were not obtained from the experiment with low conversion (ideally <5%) and no external diffusion limitation we assumed for calculations, the very low values of the Weisz-Prater criterion (close to 10^{-2}) suggest that these assumptions/simplifications are not going to change our conclusions.

3. References

1 S. Li, Q. Xu, E. Uchaker, X. Cao and G. Cao, *CrystEngComm*, 2016, **18**, 2532–2540.

2 H. N. Kim and S. K. Lee, *Geochimica et Cosmochimica Acta*, 2013, **120**, 39–64.

3 A. Takagaki, C. Tagusagawa, S. Hayashi, M. Hara and K. Domen, *Energy Environ. Sci.*, 2010, **3**, 82–93.

4 J. Datka, A. M. Turek, J. M. Jehng and I. E. Wachs, *Journal of Catalysis*, 1992, **135**, 186–199.

5 M. A. Ardagh, Z. Bo, S. L. Nauert and J. M. Notestein, *ACS Catal.*, 2016, **6**, 6156–6164.

6 P. Harriott, *Chemical Reactor Design*, CRC Press, 2002.

7 W.-L. Weng, *J. Chem. Eng. Data*, 1999, **44**, 788–791.

8 B. González, N. Calvar, E. Gómez and Á. Domínguez, *The Journal of Chemical Thermodynamics*, 2007, **39**, 1578–1588.

9 S. R. S. Sastri, S. Mohanty and K. K. Rao, *Can. J. Chem. Eng.*, 1996, **74**, 170–172.

10 M. E. Davis and R. J. Davis, *Fundamentals of chemical reaction engineering*, McGraw-Hill Higher Education, New York, NY, 2003.